Raman resonance and orientational order in fibers of single-wall carbon nanotubes

E. Anglaret,[1] A. Righi,[1,2] J. L. Sauvajol,[1] P. Bernier,[1] B. Vigolo,[3] and P. Poulin[3]
[1]*Groupe de Dynamique des Phases Condensées, UMR CNRS 5581, Université Montpellier II, France*
[2]*Departamento de Fisica, Universidade Federal de Minas Gerais, Belo Horizonte, Brazil*
[3]*Centre de Recherches Paul Pascal, UPR CNRS 8641, Université Bordeaux I, France*
(Received 23 November 2001; published 10 April 2002)

Polarized Raman spectroscopy is used to study Raman resonance and orientational order in fibers of single-wall carbon nanotubes. The polarized Raman intensity follows essentially the same angle dependence for both radial breathing mode and tangential modes and for both semiconducting and metallic nanotubes. A simple resonant model is proposed, which provides good fits of the whole vertical-vertical and vertical-horizontal data in different kinds of fibers. The model is used to describe orientational order of nanotubes in anisotropic fibers.

DOI: 10.1103/PhysRevB.65.165426 PACS number(s): 78.30.Na

I. INTRODUCTION

Control and characterization of the orientation of nanotubes in bulk materials is a major challenge for the study of physical properties (electronic, thermic, vibrational) and for applications. Several techniques have been developed by different groups to prepare anisotropic nanotube-based materials. Gommans *et al.* used an electrophoretic method to prepare fibers of single-wall carbon nanotubes (SWNT).[1] Haggenmueller *et al.* used solvent casting and melt mixing to prepare PMMA/SWNT films and a melt spinning/extrusion processing method to prepare composite PMMA/SWNT fibers (1 wt % nanotubes).[2] Smith *et al.* prepared anisotropic films by filtering suspensions of SWNT under strong magnetic fields.[3] Recently, Vigolo *et al.* developed a simple process, based on the dispersion of SWNT in surfactant suspensions followed by a recondensation of the nanotubes in the flow of a polymer solution, which makes SWNT assemble into infinitely long ribbons and fibers.[4] For all these anisotropic materials, accurate techniques for characterization of the orientational order are required. The use of birefringence techniques is limited because of strong optical absorption. Electron microscopies provide useful informations but fail to achieve an accurate quantitative description of the orientation order. X-ray diffraction has been used to study the distribution of nanotube orientations in films[3] and fibers.[5] The technique probes the orientation of two-dimensional (2D) hexagonal arrays of nanotubes assembled in bundles. Gaussian distributions with typical FWHM (full width at half maximum) of about 35° were found for the films deposited under magnetic fields.[3] The sum of a constant and a Gaussian distribution with typical FWHM about 75° was used to achieve good fits of the results for fibers prepared by recondensation of dispersed SWNT in the flow of a polymer solution.[5]

Another widely used technique to study SWNT has been Raman scattering.[1,6–15] The frequency of the radial breathing mode (RBM) is a relevant probe to estimate the diameter of SWNT.[12–14] The Raman signal is resonantly enhanced when the energy of the laser light is close to optical-absorption thresholds. For SWNT of diameter in the range 1–2 nm, this occurs in the visible and near infrared. Furthermore, absorption energies are diameter dependent and significantly shifted for metallic and semiconducting nanotubes, which makes Raman a unique probe to study selectively SWNT as a function of their diameter and metallic or semiconducting character.[12,13,15] Several groups have recently attempted to study anisotropic samples via Raman measurements.[1,6–11] Saito *et al.* calculated in a classical (nonresonant) model the intensity of the Raman lines for a single nanotube in several configurations of polarization as a function of the angle between the nanotube axis and the laser light polarization, hereafter called ϕ.[16] Rao *et al.* found that the angle dependence of the Raman intensity in VV configuration (vertical-vertical, i.e., same polarizations for incident and scattered light) for the tangential mode (TM) of aligned multiwall carbon nanotubes was well fitted by that of the A_{1g} component of the TM in the calculations.[8] Jorio *et al.* also used a nonresonant analysis to describe experimental results on aligned bundles of semiconducting SWNT.[9] They assigned two peaks measured at about 1550 and 1610 cm^{-1} to tangential modes of E_2 symmetry and two other peaks measured about 1565 and 1590 cm^{-1} to unresolved tangential modes of A_1 and E_1 symmetries. However, the samples studied were very heterogeneous and contained both SWNT with a broad diameter dispersion and multiwall carbon nanotubes (MWNT).[9,10] After subtraction of the contributions of MWNT and atypical SWNT, the authors concluded that the effect of anisotropic tube absorption (so-called ''antenna'' effect) is stronger for metallic tubes than for semiconducting ones.[10] Gommans *et al.* showed that the VV intensity of all Raman modes for metallic SWNT with a small diameter dispersion decreases continuously when the angle between fiber axis and light polarization, hereafter called Ψ, increases.[1,6] They proposed a simple resonant model where the only nonzero absorption cross section, and consequently the only nonzero component of the Raman polarizability tensor, is for light polarized parallel to the tube axis (''antenna effect'' in Ref. 10). This assumption was supported by calculations[17] and by reflectivity measurements.[6] This allowed them to describe well the angle dependence of the Raman intensity measured experimentally. However, the authors considered a 2D (in the polarization plane) disorientation of the tubes, which is incompatible with the cylindrical symmetry of fibers and leads to underestimation of the tube orientation, as shown elsewhere.[11] Duesberg *et al.* observed a similar behavior of

the Raman intensity on isolated or thin ropes of metallic SWNT and reported an angular dependence nearly proportional to $\cos^2(\phi)$ for VV intensity. Recently, Reich *et al.* investigated the phonon symmetries in the Raman spectra of nanotubes using linearly and circularly polarized light.[18] They demonstrated that for the A_1 RBM of SWNT, all components of the Raman polarizability tensor were negligible with respect to the (z,z) one where z is the axis of the tube. They also investigated the relative contributions of A_1, E_1, and E_2 components in the TM of SWNT. They found that the A_1 phonons are responsible for most of the intensity and that the (x,x) and (y,y) of the A_1 tensor represents less than 5% of the overall intensity.

Many discrepancies and questions arise from these different studies. Are the nonresonant model of Ref. 16 or the resonant model of Ref. 1 relevant to describe the experimental data for SWNT? Is the relevant model dependent on the metallic or semiconducting character of the tubes? How can one estimate accurately the distribution of tube orientation in a fiber? To address these questions, we report in this paper Raman measurements[19] performed on partially aligned fibers of well-characterized SWNT. We propose a simple model based on the hypothesis that resonant scattering for both RBM and TM modes and both metallic and semiconducting SWNT is only effective for light polarized parallel to the tube axis. We use a cylindrical orientational distribution around the tube axis and consider a correction factor to take into account light absorption from the nanotubes, which was not made in previous published models. We validate our model by fitting simultaneously five intensity ratios with only two adjustable parameters, which is also achieved for the first time to our knowledge. Furthermore, we fit the Ψ dependence of the Raman intensities in both VV and VH (vertical-horizontal, i.e., crossed polarizations for incident and scattered light) configurations. Our model offers a simple and effective way to estimate orientational order in fibers of SWNT.

II. EXPERIMENTAL

SWNT were prepared by the electric arc technique. They are characterized by a mean diameter of about 1.4 nm and a narrow diameter dispersion as determined by x-ray diffraction and Raman studies.[14,20] They were aligned in a fiber using the process developed by Vigolo *et al.*[4] Raman spectra were excited with the green line (2.41 eV) and the red line (1.92 eV) of an Ar-Kr laser in order to probe selectively the signal from semiconducting and metallic tubes, respectively.[12,13,15] Spectra were recorded in a backscattering geometry. The Raman intensities measured on different areas of the fiber were slightly different indicating some heterogeneity in the orientational order along the fiber. Therefore, each set of spectra was measured over three different areas to get a statistical picture of order in the fiber.

III. RESULTS

Typical raw data are presented in Fig. 1. The RBM frequencies are between 160 and 200 cm^{-1} which corresponds to a diameter distribution between 1.2 and 1.55 nm for nanotubes assembled in bundles.[14] For such diameters, one expects selective resonance from semiconducting tubes at 2.41 eV and from metallic tubes at 1.92 eV.[15] This is confirmed by the symmetric Lorentzian-like profile of the components of the TM at 2.41 eV and their asymmetric, broad Breit-Wigner-Fano-like profile at 1.92 eV. For VV configuration, one essentially observes an overall and continuous decrease of the Raman intensity for both RBM and TM for increasing

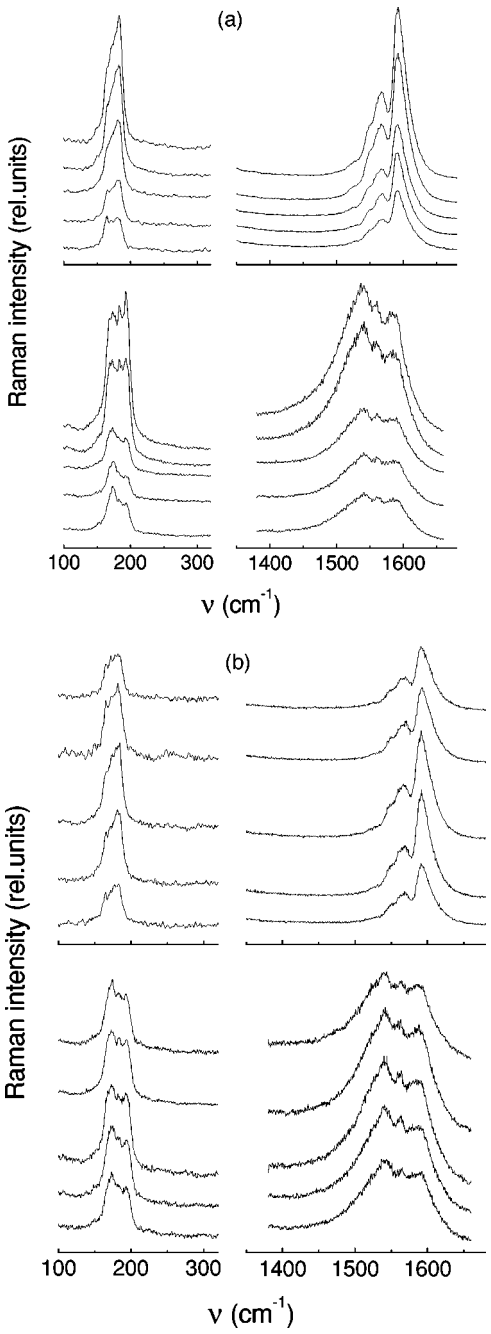

FIG. 1. Typical raw experimental Raman results (relative units) for a Vigolo fiber in VV (a) and VH (b) polarizations in the ranges of the RBM (left) and TM (right), for laser energies 2.41 eV (top) and 1.92 eV (bottom). For each figure, from top to bottom, $\Psi = 0°$, 11°, 45°, 68°, 90°.

values of Ψ. Note that the different components of the RBM and TM bunches display slightly different dependences whose origin will be discussed below. This overall decrease was already observed on fibers prepared using an electrophoretic process[1] and on isolated or thin bundles of SWNT.[7] We also observed a similar behavior on fibers prepared with nanotubes synthesized from the HiPco process,[21] which are characterized by a smaller mean diameter and a rather large diameter dispersion (about 1.05 ± 0.3 nm).[22] Therefore, this general decrease of the Raman intensity appears to be independent of the diameter and of the metallic or semiconducting character of the tubes. This is in total variance with what is expected from nonresonant calculations where, for example, the A_{1g} RBM is expected to display a minimum intensity at $\Psi = 0°$ and a maximum intensity at $\Psi = 90°$ while the main (A_{1g}) component of the TM goes through a minimum around 56°.[16] By contrast, this is in good qualitative agreement with the assumption that in the resonant Raman process the (z,z) component of the Raman polarizability tensor (where z refers to the tube axis), is much larger than all other components, as proposed in Ref. 1. This assumption is supported by optical-absorption calculations[17] and measurements on single nanotubes.[7] This is also confirmed for RBM by measurements in linearly and circularly polarized light on powders.[18] For VH configuration, one also observes a similar Ψ dependence for RBM and TM (Fig. 1). The intensity increases and goes through a maximum at 45° and then decreases symmetrically up to 90°. The two ratios $I_{\mathrm{VV},90°}/I_{\mathrm{VV},0°}$ and $I_{\mathrm{VH},0°}/I_{\mathrm{VH},45°}$ appear to be relevant probes to estimate the FWHM of the distribution of orientations. In the following, we will compare these ratios, as well as the depolarization ratios $I_{\mathrm{VH},0°}/I_{\mathrm{VV},0°}$ and $I_{\mathrm{VH},45°}/I_{\mathrm{VV},45°}$ to calculations for various distribution functions. Note that for VV configuration and $\Psi = 90°$, one expects a weak intensity for well-aligned tubes in the resonant model. By contrast, in the nonresonant model, the intensity is maximum for RBM and it goes through a secondary maximum for TM.[16] Therefore, if all components of the polarizability tensor [except the (z,z) one] are not strictly zero, the calculated ratio $I_{\mathrm{VV},90°}/I_{\mathrm{VV},0°}$ will be underestimated with respect to experiments. In order to test this possibility, we also calculated the ratio $I_{\mathrm{VV},45°}/I_{\mathrm{VV},0°}$ for each set of parameters. We will show below that comparison of calculations and data allow us to describe well orientational order in fibers.

The Ψ dependences of the Raman intensity for VV and VH measurements in the ranges of RBM and TM are displayed in Fig. 2. The rather large dispersion of the points has two main origins: (i) the inhomogeneity of orientational order along the fiber and (ii) the difference between the results obtained for the different components of RBM and TM, for red and green laser light. The first source of dispersion can be lowered in the future. As for the second source of dispersion, it shows the limits of our simple assumption that all modes for all laser energies can be associated to a same (resonant) Raman polarizability tensor. To overpass these limits and get a very accurate description of the distribution function of tube orientations, more sophisticated models should be used. However, we will show below that our simple model can provide a good general agreement of the whole data and therefore a relevant estimate of the orientational order.

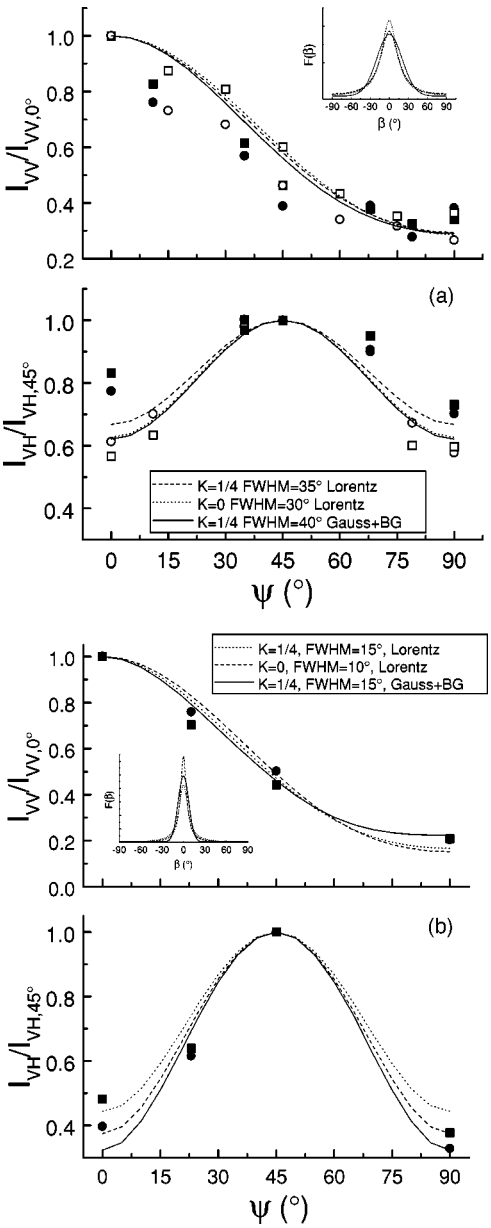

FIG. 2. Ψ dependence of the Raman intensity in VV (top) and VH (bottom) polarization configurations for (a) electric arc sample (present study), (b) data from Ref. 1. Open (solid) symbols are for laser energy 2.41 eV (1.92 eV). Squares (circles) are for RBM (TM). Lines are best fits of the experimental data (see text). Insets: corresponding distribution functions (see text for details).

IV. CALCULATION OF RAMAN INTENSITIES

Without any assumption on the Raman tensor, the scattered Raman intensity for one nanotube in the reference frame of the fiber writes:

$$I_t(\Psi) = \sum n_A n_{A'} \epsilon_{AB} \epsilon_{A'B'} E_B E_{B'},$$

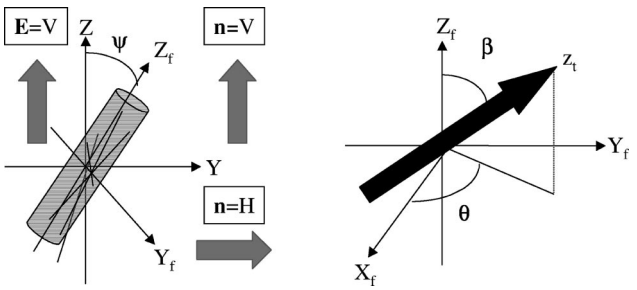

FIG. 3. Sketch of reference frames and angles. Subscript *t* is for tube, subscript *f* is for fiber, and (*X,Y,Z*) is the reference frame of the lab.

where $E_B(\Psi)$ and $n_A(\Psi)$ refer to the cartesian components of incident and scattered light vectors, respectively, and ϵ_{AB} are the components of the polarizability tensor of the tube in the referential of the fiber. The latter is a function of the components ϵ_{ab} of the Raman polarizability of the tubes in their own reference frame and of the components of the rotation matrix R that goes from the fiber frame to the tube frame:

$$\epsilon_{AB}(\beta,\theta)=\sum R_{Aa}R_{Bb}\epsilon_{ab},$$

where β is the angle between fiber axis and nanotube axis and θ is the azimuthal angle (Fig. 3). In our assumption, the only nonzero component of the Raman tensor of the nanotube is ϵ_{zz}. Consequently, the intensity scattered by one nanotube and measured in the reference frame of the lab is the sum of 16 terms:

$$I_t(\Psi,\beta,\theta)=\sum\sum n_A n_{A'} R_{Az}R_{Bz}\epsilon_{zz}\epsilon_{zz}R_{A'z}R_{B'z}E_B E_{B'}.$$

This expression of the intensity does not consider any optical correction factor. We feel justified to neglect reflection since reflectance of well-aligned SWNT fibers and mats was shown by Hwang *et al.* to be very weak in the visible range.[6] By contrast, optical absorption is not only expected to be strong but also intrinsically anisotropic. Therefore, one must consider a correction factor $f_{\rm abs}$ in the calculations taking into account the angle dependence of optical absorption, i.e., the angle dependence of the beam penetration depth. For large absorptions, $f_{\rm abs}=(\alpha_i+\alpha_s)^{-1}$ (Ref. 23), where α_i and α_s are the absorption coefficients for incident and scattered light, respectively. These coefficients express as a function of the nanotube absorption coefficients for light parallel and perpendicular to the tube axis $\alpha_\parallel$ and $\alpha_\perp$, and the angle $\phi(\Psi,\beta,\theta)$ between polarization of light and nanotube axis. Finally, we get $f_{\rm abs}=\{\alpha_\parallel[(\cos\phi_i+\cos\phi_s)+K(\sin\phi_i+\sin\phi_s)]\}^{-1}$ with $K=\alpha_\perp/\alpha_\parallel$. In order to calculate the intensity scattered by the fibers, one has to weight the intensity for each tube by a distribution function $F(\beta)$ of the orientation and integrate the result over the whole space:

$$I_f=\int_0^\pi\int_0^{2\pi} I_t f_{\rm abs}F(\beta)\sin\beta\,d\beta\,d\theta.$$

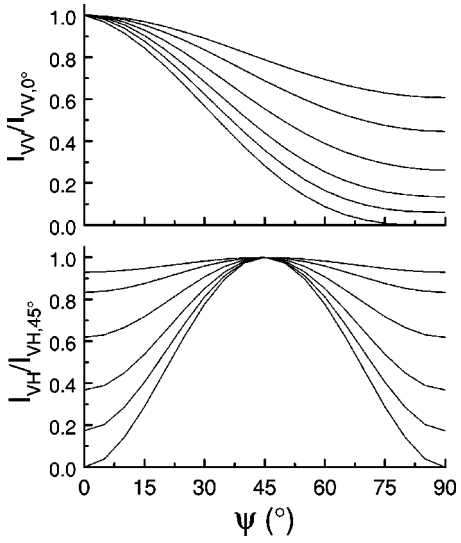

FIG. 4. Ψ dependence of the calculated intensity for VV (top) and VH (bottom) polarizations, for a Lorentzian distribution function with FWHM of 0°, 1°, 10°, 30°, 60°, and 90° (from bottom to top). The results for 0° correspond to calculations for a single tube.

For the distribution function, this is reasonable to assume that the function presents a cylindrical symmetry and goes through a maximum for $\beta=0$ and $\beta=\pi$. We used the sum of two Lorentzian (or Gaussian) functions with the same profile, centered on $\beta=0$ and $\beta=\pi$, suitably normalized to describe 3D disorientation relevant for fibers. Therefore, in our calculations, there are only two adjustable parameters: FWHM of the distribution function and the absorption anisotropy constant *K*. Typical examples of calculations are displayed in Fig. 4 for $K=1/4$ and various values of FWHM for a Lorentzian distribution. As expected, the VV intensity decreases continuously from 0° to 90° and the VH intensity goes through a maximum at 45° and decreases on both sides symmetrically down to 0° and 90°. The narrower the FWHM of the distribution function and the faster the decrease. To determine the unknowns FWHM and *K* from the data, we will consider five relevant polarization ratios: $I_{\rm VV,90°}/I_{\rm VV,0°}$, $I_{\rm VV,45°}/I_{\rm VV,0°}$, $I_{\rm VH,45°}/I_{\rm VH,0°}$, $I_{\rm VH,0°}/I_{\rm VV,0°}$, and $I_{\rm VH,45°}/I_{\rm VV,45°}$ where the subscript refers to the polarization configuration and the angle Ψ. Note that the unknowns ϵ_{zz} and $\alpha_\parallel$ eliminate in these ratios. Note also that the isotropic depolarization ratio, i.e., the polarization ratio for a powder, provides an additional independent constant. In the present case, it gives a justification to neglect all the components of the Raman polarizability tensor. Finally, note that we also run calculations for (i) 2D disorientation (tube axis in the polarization plane) and/or (ii) without considering any absorption coefficient factor, in order to compare our results with those of Ref. 6.

V. DISCUSSION

For us, the relevant test to validate calculations will be to fit the five ratios with the same set of parameters (FWHM, *K*). In Fig. 5, we report the results of calculations for 3D disorientation (cylindrical symmetry), for Lorentzian and

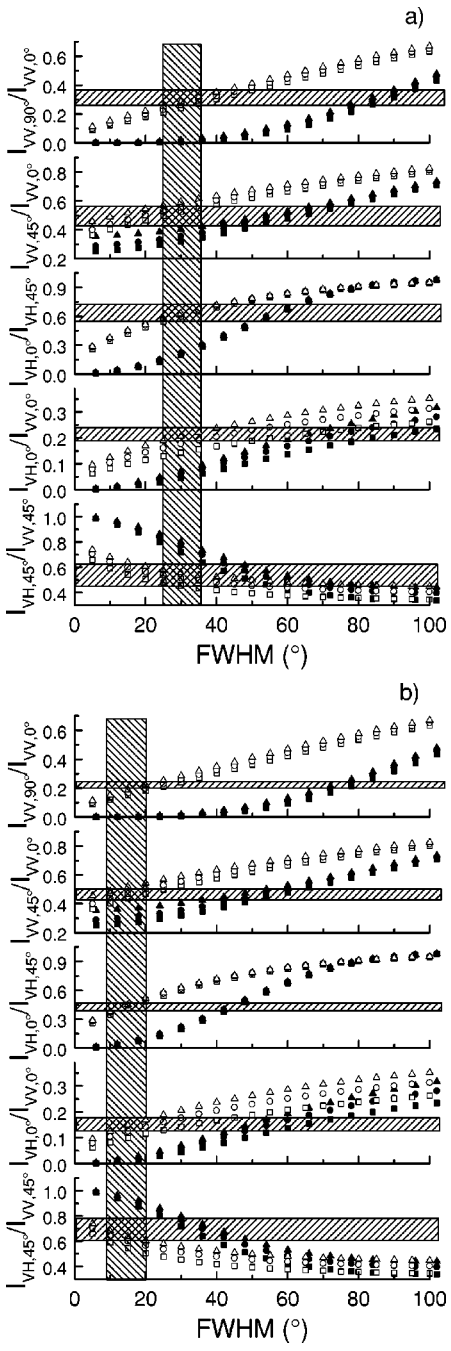

FIG. 5. FWHM dependences of the five intensity ratios for Lorentzian (open symbols) and Gaussian (solid symbols) distributions. No absorption was considered for squares, $K=1/4$ for circles and $K=0$ (absorption only for polarization parallel to tube axis) for triangles. Horizontal hatched areas correspond to experimental values for (a) electric arc sample (present study), (b) data from Ref. 1. Vertical hatched areas indicate the values of FWHM providing the best fit of all the intensity ratio simultaneously for Lorentzian distributions (see text).

Gaussian functions, and for different values of the absorption anisotropy constant K, as a function of the FWHM of the distribution function. Note that the results appear significantly different for Lorentzian and Gaussian functions, especially for small values of FWHM. This relates to the strong contribution of the ''tail'' of the Lorentian function for $\Psi=90°$ and $\Psi=0°$ in VV and VH configurations, respectively. The experimental ratios were calculated for RBM and TM and for the two laser lines for the Vigolo fiber. The dispersion for each value of Ψ for a given sample is between 5% and 30%, which corresponds to dispersion between the results for different modes, different laser lines, and different areas. The horizontal hatched areas correspond to the experimental ratio for the present data [Fig. 5(a)] and for data of Ref. 1 [Fig. 5(b)]. First, note that no agreement can be found simultaneously for the five ratios when considering planar (2D) disorientation and a Lorentz function (not shown, see discussion and some results in Ref. 11). For 3D disorientation with a cylindrical symmetry, good fits of the whole set of data occurs only for Lorentzian distributions of orientations (vertical hatched areas in Fig. 5). For the Vigolo fiber, this is achieved for a FWHM of $30°\pm5°$. For data of Ref. 1, the distribution of orientations is narrower, with a FWHM of $15°\pm5°$. Best fits are obtained for small values of K (triangles and circles in Fig. 5) indicating strongly anisotropic absorption, as expected. By contrast, no simultaneous fit of the five ratios can be achieved for Gaussian distributions of orientations. Indeed, the contribution of the ''tail'' of the Lorentzian appears to be essential to achieve good fits. Another way to interpret this is to consider that the fibers contain a mixture of oriented and unoriented tubes. Such an assumption was already made in Ref. 1 and the presence of unoriented tubes was also evidenced by the x-ray-diffraction (XRD) results of Ref. 5. Therefore, the key for a good fit with a Gaussian distribution would be to add a background (BG), where the BG corresponds to unoriented tubes in the samples. Note that for a Lorentzian, the weight of the function at $\beta=\pi/2$ accounts for such a background. Satisfactory results are obtained for a FWHM of 40° and a rate of unoriented tubes of 1/5 for the Vigolo fiber, and for a FWHM of 15° and a rate of unoriented tubes of 1/6 for results of Ref. 1. This is amazing to observe that this ratio of unoriented tubes is very close to that determined by Gommans *et al.* for the same data with a model assuming one part ($p=0.86$) of the nanotubes uniformly oriented between 0° and an angle θ and the other part ($1\text{-}p=0.14$, very close to our 1/6) uniformly (mis)oriented between θ and (π-θ). Note that θ was determined using a 2D model and can therefore not be compared directly to our results. The best fits of the Ψ dependence of the Raman intensity in the fibers are reported in Fig. 2. The corresponding distribution functions are presented in the insets. Note that the ''tails'' of the functions are comparable for the Lorentzians and the sums (Gaussian+BG).

Good fits are achieved for both VV and VH results. A much better accuracy on the calculations would be expected by considering additional (weak and mode-dependent) components of the polarizability tensor and by considering different K parameters for metallic and semiconducting tubes. For example, let us consider not strictly nonzero values for the other components of the Raman tensor. For a mode of A_{1g} symmetry, the (x,x) and (y,y) components of the Raman tensor are, with the (z,z) one, the only nonzero components values expected in a nonresonant model. In the case of RBM, each peak in the bunch corresponds to a different tube diam-

eter. If the (x,x) and (y,y) components are not strictly zero, their relative value, with respect to that of the (z,z) component, will likely depend on diameter and possibly on chiral angle. This would explain the slightly different Ψ dependences of the different components of the RBM in Fig. 1(a). In the case of TM, the different peaks in the bunch do not correspond to different tube diameters but to modes of different symmetries, associated with different polarizability tensors. Therefore, small but nonzero values of some components of the tensors would also explain the slightly different Ψ dependences of the different components of the TM in Fig. 1(a). Note that the problem is less critical for VH configuration since the expected Ψ dependences for resonant and nonresonant models are close to each other for the A_{1g} components of both RBM and TM. Despite these imperfections, one can observe that a good overall description of the data is achieved. Therefore, our model provides a simple and useful way to estimate orientational order in fibers of SWNT from Raman measurements. We claim that Lorentzian distributions of tube orientations with FWHM of $30° \pm 5°$ and $15° \pm 5°$ give a good picture of tube orientations in fibers prepared from the process described in Refs. 4 and 1, respectively. Gaussian distributions of tube orientations with the same FWHM also allow us to fit the data, providing that one considers a significant part of unoriented tubes. We also underline that both the ratios $I_{VV,45°}/I_{VV,0°}$ and $I_{VV,90°}/I_{VV,0°}$ must be considered to estimate the distribution of tube orientations. A first estimation based on the ratio $I_{VV,90°}/I_{VV,0°}$ only led to FWHM of $40° \pm 5°$ and $20° \pm 5°$ for the same samples,[11] slightly overestimated with respect to the present values. Finally, it is interesting to compare these results to diffraction results. Launois *et al.* found that the best fit of their data for other fibers prepared from the Vigolo process was achieved with the sum of a Gaussian function with FWHM of $75° \pm 5°$ and a constant that corresponds in part to the contribution of unoriented tubes.[23] The assumption that a part of the tubes is unoriented is necessary in both cases to achieve good fits with Gaussian distribution functions, but the fitted FWHM is very different. This may indicate that the orientation of the tubes in the fibers is very sensitive to the details of the preparation process and therefore very different from the fibers studied in XRD and Raman but this is unlikely since XRD results were fairly reproducible for many different fibers.[24] We rather believe that the differences can be explained by the specificities of each technique. First, the analysis of Ref. 5 considered the diffraction peak (10) and was therefore sensitive to the orientation of bundles of tubes. By contrast, one probes all tubes in Raman experiments. If a significant part of the tubes is individual or in small and/or ill-crystallized bundles, which is possibly the case given the weak intensity of the (10) peak in Ref. 5, the smallest FWHM measured in Raman would indicate that individual tubes or small bundles are better oriented than large and well-crystallized bundles. However, the most likely explanation for the difference between XRD and Raman results is that XRD probes the whole thickness of the fiber, while optical absorption restricts the effective thickness in Raman to a few microns at most. If the orientation of the fibers is not homogeneous between surface and center, one expects differences between XRD and Raman results. In the future, we will have to test more systematically the correlation between XRD and Raman by working on the same samples.

VI. CONCLUSION

Polarized Raman spectroscopy was used to study orientational order and resonance in fibers of SWNT. We state that for convenient excitation energy (close to an optical transition of the tubes), the angle dependence of the Raman intensity for both semiconducting *and* metallic nanotubes cannot be interpreted in a nonresonant model. A simple resonant model assuming that the (z,z) component of the Raman polarizability tensor is much larger than all other components for all Raman modes (and in particular for RBM and TM) leads to a good agreement with the measured intensity ratios and satisfactory fits of the angle dependence of the Raman intensities. Lorentzian distributions of orientations with typical FWHM of 35° and 15° were found for fibers prepared by condensation of nanotubes in the flow of a polymer solution and by an electrophoretic method, respectively.

ACKNOWLEDGMENT

We gratefully acknowledge Pascale Launois for stimulating interactions and pertinent comments on the manuscript.

[1] H. H. Gommans, J. W. Alldredge, H. Tashiro, J. Park, J. Magnuson, and A. G. Rinzler, J. Appl. Phys. **88**, 2509 (2000).

[2] R. Haggenmueller, H. H. Gommans, A. G. Rinzler, J. E. Fischer, and K. I. Winey, Chem. Phys. Lett. **330**, 219 (2000).

[3] B. W. Smith, Z. Benes, D. E. Luzzi, J. E. Fischer, D. A. Walters, M. J. Casavant, J. Schmidt, and R. E. Smalley, Appl. Phys. Lett. **77**, 663 (2000).

[4] B. Vigolo, A. Pénicaud, C. Coulon, C. Sauder, R. Pailler, C. Journet, P. Bernier, and P. Poulin, Science **290**, 1331 (2000).

[5] P. Launois, A. Marucci, B. Vigolo, P. Bernier, A. Derr, and P. Poulin, J. Nanoscience Nanotech. **1**, 125 (2001).

[6] J. Hwang, H. H. Gommans, H. Tashiro, R. Haggenmueller, K. I. Winey, J. E. Fischer, D. B. Tanner, and A. G. Rinzler, Phys. Rev. B **62**, R13310 (2000).

[7] G. S. Duesberg, I. Loa, M. Burghard, K. Syassen, and S. Roth, Phys. Rev. Lett. **85**, 5436 (2000).

[8] A. M. Rao, A. Jorio, M. A. Pimenta, M. S. S. Dantas, R. Saito, G. Dresselhaus, and M. S. Dresselhaus, Phys. Rev. Lett. **84**, 1820 (2000).

[9] A. Jorio, G. Dresselhaus, M. S. Dresselhaus, M. Souza, M. S. S. Dantas, M. A. Pimenta, A. M. Rao, C. Liu, and H. M. Cheng, Phys. Rev. Lett. **85**, 2617 (2000).

[10] C. Fantini, M. A. Pimenta, M. S. S. Dantas, D. Ugarte, A. M. Rao, A. Jorio, G. Dresselhaus, and M. S. Dresselhaus, Phys. Rev. B **63**, 161405 (2001).

[11] E. Anglaret, A. Righi, J. L. Sauvajol, P. Bernier, B. Vigolo, and P.

Poulin, in *Proceedings of CNT10, Tsukuba, Japan, 2001*, edited by S. Iijima, S. Saito, M. Yudasaka, and Y. Miyamoto.
[12] M. S. Dresselhaus and P. C. Eklund, Adv. Phys. **49**, 705 (2000), and references therein.
[13] J. L. Sauvajol, E. Anglaret, S. Rols, and L. Alvarez, Carbon (to be published), and references therein.
[14] S. Rols, A. Righi, L. Alvarez, E. Anglaret, C. Journet, P. Bernier, J. L. Sauvajol, A. M. Benito, W. K. Maser, E. Munoz, M. T. Martinez, G. F. de la Fuente, A. Girard, and J. C. Ameline, Eur. Phys. J. B **18**, 201 (2000).
[15] M. A. Pimenta, A. Marucci, S. A. Empedocles, M. G. Bawendi, E. B. Hanlon, A. M. Rao, P. C. Eklund, R. E. Smalley, G. Dresselhaus, and M. S. Dresselhaus, Phys. Rev. B **58**, R16016 (1998).
[16] R. Saito, T. Takeya, T. Kimura, G. Dresselhaus, and M. S. Dresselhaus, Phys. Rev. B **57**, 4145 (1998).
[17] H. Ajiki and T. Ando, Physica B **201**, 349 (1994).
[18] S. Reich, C. Thomsen, G. S. Duesberg, and S. Roth, Phys. Rev. B **63**, 041401 (2001).
[19] H. Sun, Z. Tang, J. Chen, and G. Li, Solid State Commun. **109**, 365 (1999).
[20] S. Rols, R. Almairac, L. Henrard, E. Anglaret, and J. L. Sauvajol, Eur. Phys. J. B **10**, 263 (1999).
[21] A. Righi *et al.* (unpublished results).
[22] P. Nikolaev, M. J. Bronikowski, R. K. Bradley, F. Rohmund, D. T. Colbert, K. A. Smith, and R. E. Smalley, Chem. Phys. Lett. **313**, 91 (1999).
[23] G. Masetti, E. Campani, G. Gorini, R. Tubino, P. Piaggio, and G. Dellepiane, Chem. Phys. **108**, 141 (1986).
[24] P. Launois (private communication).